# Reconstruction of Complexly Encoded Images

By R. C. PUETTER[1]

[1]Center for Astrophysics and Space Sciences,
University of California, San Diego
9500 Gilman Drive
La Jolla, CA, 92093-0111, USA
rpuetter@ucsd.edu

This lecture explores the application of pixon-based methods to the reconstruction of complexly encoded images. The special problems sometimes associated with complexly encoded data sets, i.e. an extremely complex and convoluted solution space, are discussed, and numerical methods for dealing with these problems, e.g. simulated annealing, genetic algorithms, and evolutionary programing, are presented. Several sample reconstructions provide examples of reconstructions of complexly encoded images using both standard multi-dimensional minimization techniques and stochastic search methods.

## 1. Introduction

This lecture concentrates on image reconstruction, i.e. deducing the spatial structure and intensity distribution of an underlying source from a data set in which the source structure and brightness are encoded in a complex manner. Examples of complexly encoded data include (1) radio interferometry in which the source brightness is encoded in a sparsely sampled interferogram, (2) medical CAT scans and ultrasound images in which the spatial structure of a patient's brain, heart, or other organs are studied by scanning a source of radiation, and recording the transmission or echo of this radiation, and (3) LIDAR, RADAR, and SONAR imaging in which reflected light or sound is used to encode the spatial structure of a field of objects in front of broadcasting antennae. These are only a few examples of the many important applications of reconstruction of complexly encoded images.

An especially important aspect of image reconstruction in the case of complexly encoded images is the high degree of ambiguity that may be encountered in solution space. In the astronomical radio interferometry imaging problem, for example, the spatial Fourier components of the image are very incompletely sampled. This means a direct inversion of the problem is impossible. Too many Fourier components are absent. Thus in order to find a solution, one is forced to provide some sort of "regularization" for the problem, e.g. making a plausible limited physical model and estimating its parameters. It is not surprising, therefore, that successful methods of radio interferometry are characterized by approaches such as CLEAN, in which the radio image is successively approximated in terms of point sources, and Maximum Entropy (ME) methods, in which the regularization is provided by insisting on a very smooth underlying source distribution.

Because of the great ambiguity in the solution of such problems, Bayesian methods are a natural choice for a solution method. They do not attempt to perform an exact inversion of the problem (which is generally impossible), but use all of the available information to constrain the range of solutions and then select the most likely solution given what is known. Indeed, the complexly encoded image problem is an excellent showcase for the power of Bayesian priors. In such cases simple Goodness-of-FIT (GOF) or Maximum

Likelihood (ML) methods usually fail miserably—such methods avoid priors. The GOF and ML criteria used simply do not adequately constrain the solution. Consequently these methods often select unphysical or non-sensical solutions since such solutions represent the typical element of solution space.

To find valid solutions to the complexly encoded image problem one must apply realistic and powerful constraints. As mentioned above, Bayesian methods are often employed for this purpose since they don't attempts to directly invert the problem, yet they make use of all of the information available to constrain the solution. Even so, the range of possible solutions can be much too large without further constraints. ME methods, for example, add the additional constraint that the solution have "maximal smoothness". The CLEAN algorithm insists on building radio images from collections of point sources. The ME method is generally too naive, while the CLEAN algorithm is much too restrictive, and suffers the typical problems associated with parametric fitting when the model is inappropriate. (A parametric fitting procedure assumes a fixed model which is characterized by a small set of parameters. The data is then used to fit the parameters.) What we require is a powerful and flexible non-parametric fitting procedure. (Non-parametric fitting attempts to model an underlying function without reference to a particular functional form. This really amounts to modeling the underlying function by using a large number of parameters—see, for example, Heden 1975; Sprent 1981; and Hardle 1990.)

Pixon-based image reconstruction is a non-parametric modeling approach for the image reconstruction problem. The language used to model the image (e.g. the pixon shape functions in the case of multiresolution pixons) is the large space of possible parameters out of which the model for the underlying image will be constructed. The GOF criterion and minimization of the Algorithmic Information Content (AIC) of the image model are the criteria by which the specific non-parametric model is selected. As argued in Lectures 2 and 3, minimization of the AIC is an ideal criterion for selecting a model to constraint a reconstruction, and use of a multiresolution language should provide a concise expression for the AIC with a resulting highly optimized Bayesian prior.

While the above arguments indicate that Bayesian methods in general, and pixon-based methods in particular, provide an excellent approach for "phrasing" or formulating the problem of reconstruction, the question of how to numerically find the solutions is still an open issue. In the case of image restoration, standard multi-dimensional optimization methods seem to work fine. This is largely because the data and the image are very closely related. Indeed, often the data is used directly as the image value, i.e. often image restoration is not even performed. In any event, if image restoration is desired, in this case the data provides an excellent first guess for the image value, and only modest extrapolations are required from this first guess to find a statistically acceptable solution. Things are much different in the case of complexly encoded images. Here the data does not provide a good first guess for the image. Indeed, it may be impossible to easily obtain a good first guess for the image. Furthermore, because of the nature of the encoding process, or incomplete sampling, or other loss of information, there is often great ambiguity in solution space. This presents an exceedingly difficult challenge for numerical methods. Thus before presenting sample reconstruction for the complexly encoded image case, it is appropriate to discuss numerical methods.

## 2. Robust Numerical Methods for Inverse Problem Solution

Large ambiguity in the solution to an optimization problem essentially means that there are many local extrema for the problem and that solution space is very "convoluted". Hence simple optimization approaches, such as the method of steepest decent

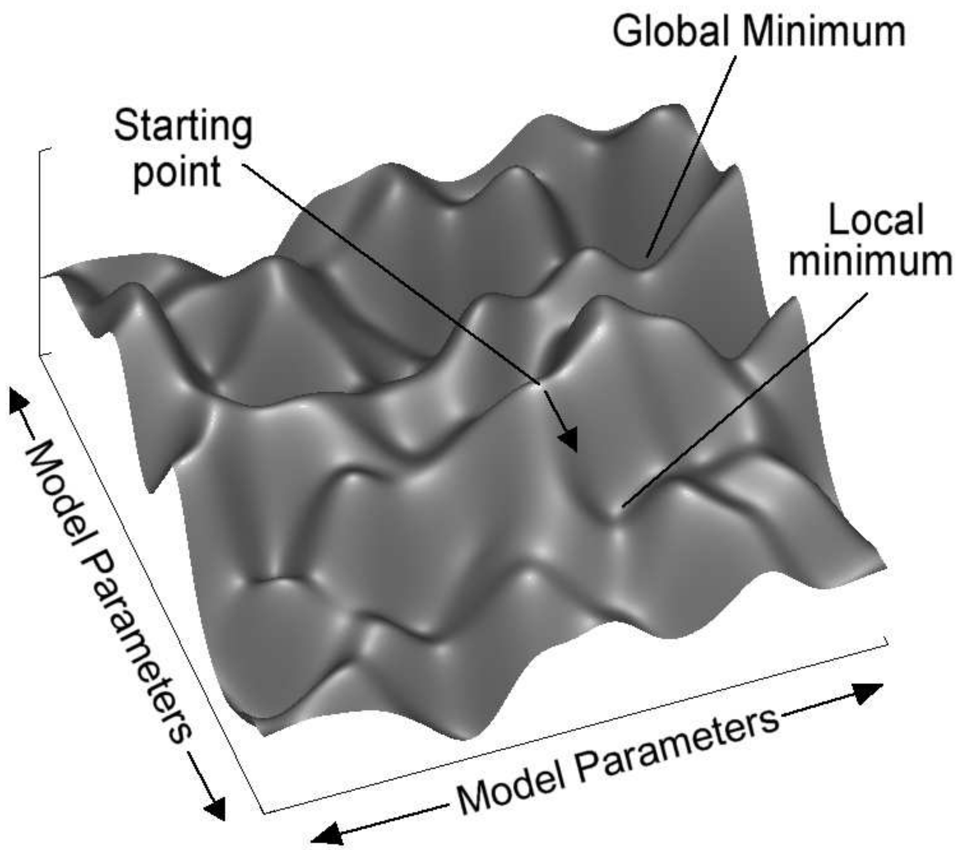


FIGURE 1. Sample solution space for the complexly encoded image reconstruction problem. There are many local extreme (illustrated here as minima) to examine before finding the globally optimal solution. Simple methods, such as the method of steepest decent, get caught in local extrema before finding the global extrema. Shown is the location of the global minimum, a sample starting point for a solution algorithm, and the direction of the gradient (direction of steepest descent).

(multi-dimensional Newton-Ralpson iteration), have an extremely small radius of convergence. (Press et al. 1994 presents an excellent discussion of the "standard" algorithms and their general convergence properties). An example of the type of solution space "terrain" that we have in mind appears in Figure 1.

As can be seen in Figure 1, the sample solution space we have selected is filled with many local extrema (we shall assume from here on that we are attempting to solve a minimization problem). Our goal is to find the *global* minimum. However, if the method of steepest descent is used as the solution algorithm, the resulting answer depends strongly on the starting point. As illustrated in the figure, proceeding down the gradient from the marked starting point results in finding a local minimum which is separated by many "hills" and "valleys" from the true global minimum.

While one can immediately see the problems with steepest descent methods, other methods, which are usually more robust, also fail if the solution space terrain is sufficiently complex. These techniques include conjugate gradient methods (which currently is our standard minimization technique for pixon-based reconstruction) and variable metric methods. Conjugate gradient methods use information on the local gradient to search for a solution, but insist at each point that the search proceeds in a direction perpendicular to the last search direction. Variable metric methods have a similar strategy, i.e. using past search directions to speed the solution. However both methods effectively assume that the function to be minimized is well approximated by a quadratic form. This, of course, will be true for almost all problems sufficiently close to the solution. (This is the case in Figure 1, too.) The practical difficulty is that one may have no way in which to get *sufficiently close* to the solution in a first guess. The starting point indicated in Figure 1 is clearly not *sufficiently close*.

As mentioned above, some image reconstruction methods try to circumvent the problem of small radii of convergence by adding mathematical constraints which *regularize* the problem, i.e. make the problem *convex* by increasing the range over which the function is well approximated by a quadratic form. Adding the ME prior often performs this feat for $\chi^2$ minimization problems, and ME is often said to regularize the image reconstruction problem. The pixon-prior also performs this function very well in most cases. However, it is not uncommon to see the ME prior fail in the complexly encoded image case, and we have seen at least one situation (and expect many others) in which the pixon prior was totally inadequate for increasing the radius of convergence of the conjugate gradient method in a practical way—see the example of the OSSE Virgo Survey data below.

In order to effectively search for the global extrema in complex solution spaces, a different approach is required. Recently, great success has been achieved for such problems by using stochastic search methods. Such methods include simulated annealing (Cerny 1982; Kirkpatrick et al. 1983; Kirkpatrick 1984; German and German 1984), genetic algorithms (Fraser 1957a; Fraser 1957b; Fraser 1968; Holland 1969; Holland 1975), and evolutionary programing (Conrad 1974; Kampfner and Conrad 1983; Conrad 1984; Conrad 1988). (An excellent review of genetic and evolutionary algorithms can be found in Fogel 1995.) Powerful mathematical theorems have been proven for these methods that show that provided that the annealing schedule is slow enough, or the evolutionary process is carried out long enough in the presence of random mutation, the resulting answer will be the globally optimal solution. While a globally optimal solution is guaranteed with these methods provided that sufficient care is taken, it is by no means guaranteed that the solution will be obtained in a computationally acceptable time, and it is how such algorithms can be made fast and efficient where significant current research effort is being applied.

In the examples presented below, we have used both standard multi-dimensional optimization methods (conjugate gradient) as well stochastic approaches (simulated annealing) to solve the image reconstruction problem. Even for the more standard methods, however, we have introduced a partial annealing process, i.e. we start with large pixon scales and gradually introduce smaller scales as the iterations proceed. Furthermore, this annealing process was found to be essential for developing a robust algorithm—see Lecture 3.

## 3. Sample Reconstructions of Complexly Encoded Images

This section presents three examples of pixon-based reconstruction of complexly encoded images. Each of these examples have been presented before (see Puetter 1995). The first example is from the $60\mu m$ survey scans of the IRAS satellite and reconstructs the image of the interacting galaxy pair M51. This example first appeared in print in Puetter and Piña 1993a. The second example is from coded aperture X-ray imaging made with the HXT instrument on the Yohkoh satellite (see Metcalf et al. 1996). The final example is of OSSE Virgo Survey data (see Dixon et al. 1996).

### 3.1. *60 Micron IRAS Survey Scans of M51*

In Figure 2 we present a reconstructed image from $60\mu m$ IRAS survey scans of the interacting galaxy pair M51. This particular data set is especially useful for comparing the performance of various different image reconstruction techniques since it was chosen as the basis of an image reconstruction contest at the 1990 MaxEnt Workshop (Bontekoe 1991). Furthermore, the IRAS data for this object is particularly strenuous for image reconstruction methods. This is because all the interesting structure is on "sub-pixel scales" (IRAS employed relatively large, discrete detectors—1.5 *arcmin* by 4.75 *arcmin* at $60\mu m$) and the position of M51 in the sky caused all scan directions to be nearly parallel. This means that reconstructions in the cross-scan direction (i.e. the 4.75 *arcmin* direction along the detector length) should be significantly more difficult than in the scan direction. In addition, the point source response of the 15 IRAS $60\mu m$ detectors (pixel angular response) is known only to roughly 10% accuracy, and finally, the data is irregularly sampled.

In Figure 3, our FPB reconstruction is compared to the results from other methods, including the Lucy-Richardson, the Maximum Correlation Method (MCM)—see Rice 1993, and MEMSYS 3 reconstructions (Bontekoe et al. 1991). The winning entry to the MaxEnt 90 image reconstruction contest was produced by Nick Weir of Caltech and is not presented here since quantitative information concerning this solution has not been published—however, see Bontekoe 1991 for a gray-scale image of this reconstruction. Nonetheless, Weir's solution is qualitatively similar to Bontekoe's solution. Both were made with MEMSYS 3. Weir's solution, however, used a single correlation length channel in the reconstruction. This constrained the minimum correlation length of features in the reconstruction, preventing break-up of the image on smaller size scales. This is probably what resulted in the "winning-edge" for Weir's reconstruction in the MaxEnt 90 contest (Weir 1993).

As can be seen from Figure 3, our FPB-based reconstruction is superior to those produced by other methods. The Lucy-Richardson and MCM reconstructions fail to significantly reduce image spread in the cross-scan direction, i.e. the rectangular signature of the 1.5 by 4.75 *arcmin* detectors is still clearly evident, and fail to reconstruct even gross features such as the "hole" (black region) in the emission north of the nucleus—this hole is clearly evident in optical images of M51. The MEMSYS 3 reconstruction by Bontekoe is significantly better. This image clearly recovers the emission "hole" and resolves the north-east and south-west arms of the galaxy into discrete sources. Nonetheless, the level of detail present in the FPB reconstruction is clearly absent, e.g. the weak source centered in the emission hole (again, this feature corresponds to a known optical source).

To assess the significance of the faint sources present in our FPB reconstruction, our reconstruction in Figure 2 is overlaid with the 5 GHz radio contours of van der Hulst et al. (van de Hulst et al. 1988). The radio contours are expected to have significant, although imperfect, correlation with the far infrared emission seen by IRAS. Hence a comparison of the two maps should provide an excellent test of the reality of structures found in our reconstruction. Also identified in Figure 2 are several prominent optical sources and (hydrogen Balmer line emission) knots. As can be seen, the reconstruction indicates excellent correlation with the radio. The central region of the main galaxy and its two brightest arms align remarkably well, and the alignment of the radio emission from the north-east companion and the IRAS emission is excellent. Furthermore, for the most part, whenever there is a source in the reconstruction which is not identifiable with

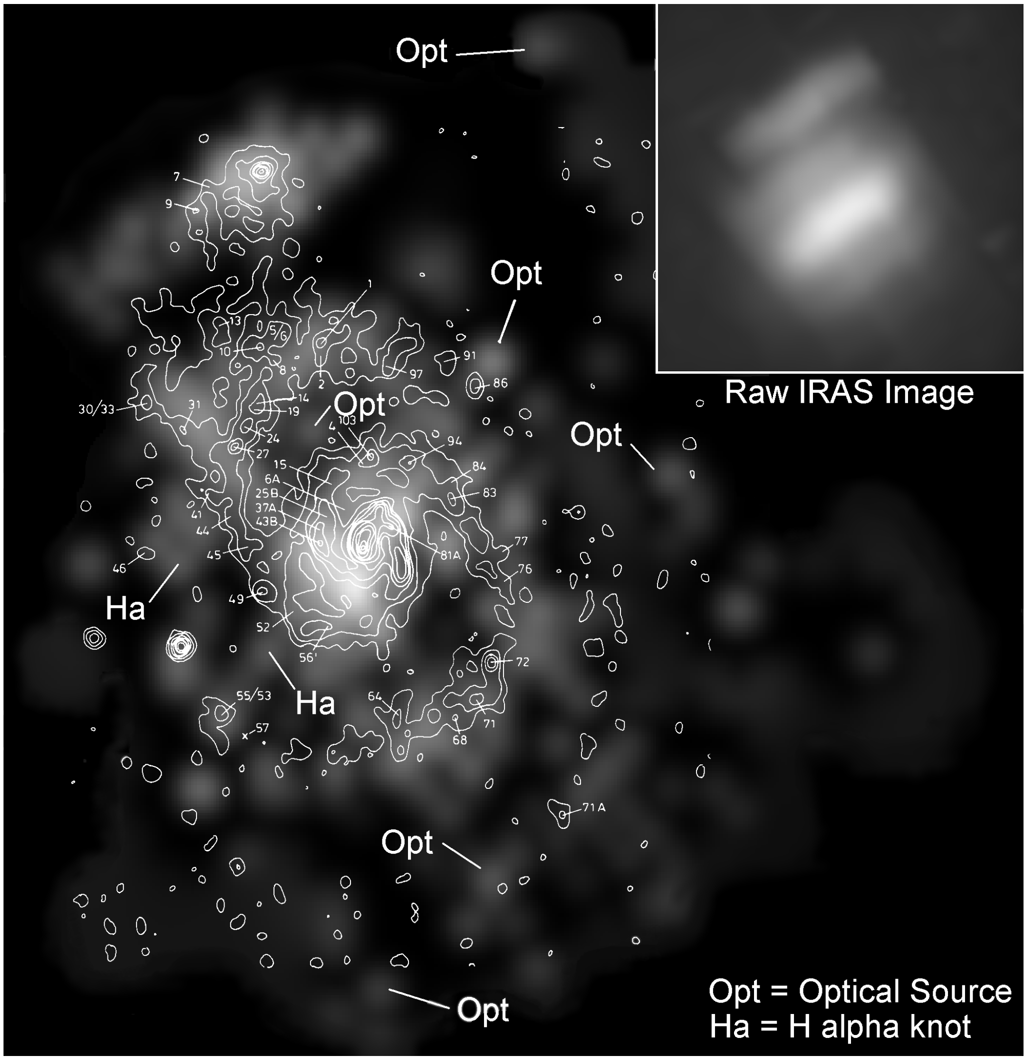


FIGURE 2. Pixon-Based reconstruction of $60\mu m$ survey scans of M51. Grey-scale image: The pixon-based reconstruction. The faintest sources visible have a formal SNR of roughly 30. Contours: The 5 $GHz$ radio flux contours of van de Hulst 1988. Noted are several of the stronger features in the reconstruction that can be indentified with optical sources (labeled "Opt") and $H\alpha$ knots (labeled "$H\alpha$"). Figure reproduced from Puetter and Piña 1993b.

a radio source, it can be identified with either optical or knots. An excellent example is the optical source in the "hole" of emission to the north-east of the nucleus of the primary galaxy or the bright optical source to the north-west of the nucleus (both labeled "Opt" in Figure 2). Because of the excellent correlation with the radio, optical, and images, we are quite confident that all of the features present in our reconstruction are real. (The faintest sources visible in Figure 2 have a formal SNR of 30.)

### 3.2. *HXT Solar Flare Imaging*

We next present a sample image reconstruction of coded mask X-ray data from the Hard X-ray Telescope (HXT) instrument on board the Yohkoh spacecraft (Kosugi et al. 1991). Figure 4 shows hard X-ray (23-33 $keV$) images of a solar flare which occurred on 20

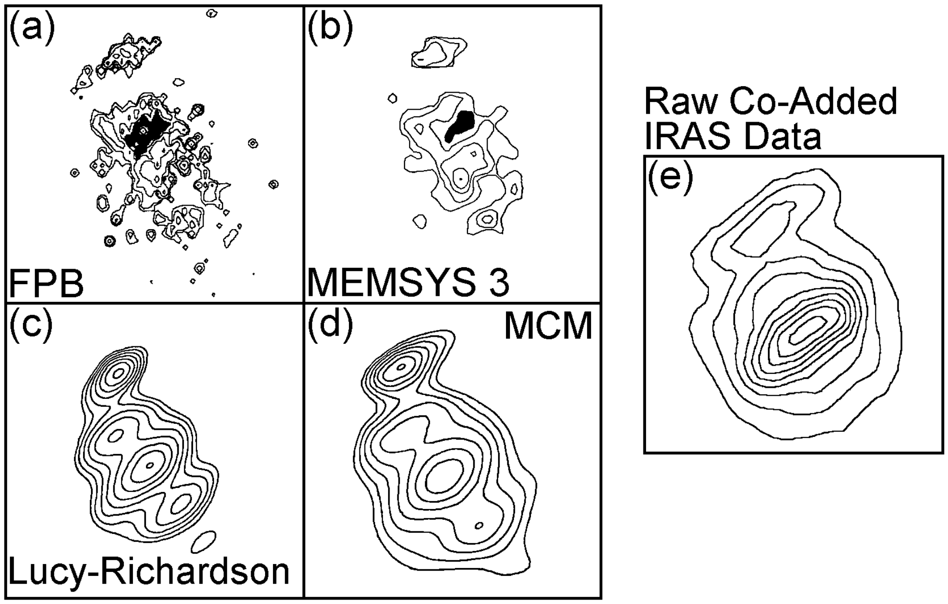


FIGURE 3. Comparison of the performance of various image reconstruction methods for the M51 IRAS survey data. Shown are the results for our pixon-based method (fuzzy, radially symmetric pixons), the Lucy-Richardson method, the "in-house" IPAC Maximum Correlation Method (MCM), and the Maximum Entropy Method (MEMSYS 3). Panel (b) is reproduced from Bontekoe 1991b by permission of the author, and panels (c) and (d) are reproduced from Rice 1993 by permission of the author. This figure first appeared in Puetter and Piña 1993a.

August 1992. Since there is no effective method of manufacturing optics with which to focus hard X-ray light, the HXT instrument takes X-ray images by taking pictures through a series of coded masks. The series of coded images is then inverted to yield the underlying source structure. Figure 4 shows a time series of 3 images. Each row of panels shows three different reconstructions. All inversions were performed by Tom Metcalf (U. Hawaii). As can be seen, direct linear inversion produces an enormous amount of spurious structure. In addition to hiding low contrast features, the presence of such spurious structure is particularly worrisome since the flux conserving nature of the algorithm requires that flux placed in spurious sources must come from the true sources thereby grossly affecting photometry. In this regard, the ME and FPB reconstructions can be seen to be a great improvement over the direct linear inversion. Relative to the pixon-based reconstruction, however, the ME inversion still produces a wealth of spurious emission, resulting in poor photometry and often over resolves real features. (We know the resolution of the ME image is too high since the quality of the pixon fit is just as good—in fact slightly better for these images—and uses a lower resolution. Hence the ME resolution is unjustified.)

### 3.3. *OSSE Gamma-Ray Imaging Toward Virgo*

As a final example of pixon-based image reconstruction, we present a comparison of two image reconstruction techniques using 50 to 150 $keV$ data from the Oriented Scintillation Spectrometer Experiment (OSSE) aboard the Compton Gamma-Ray Observatory (GRO). The OSSE instrument consists of four shielded detectors with a field of view of

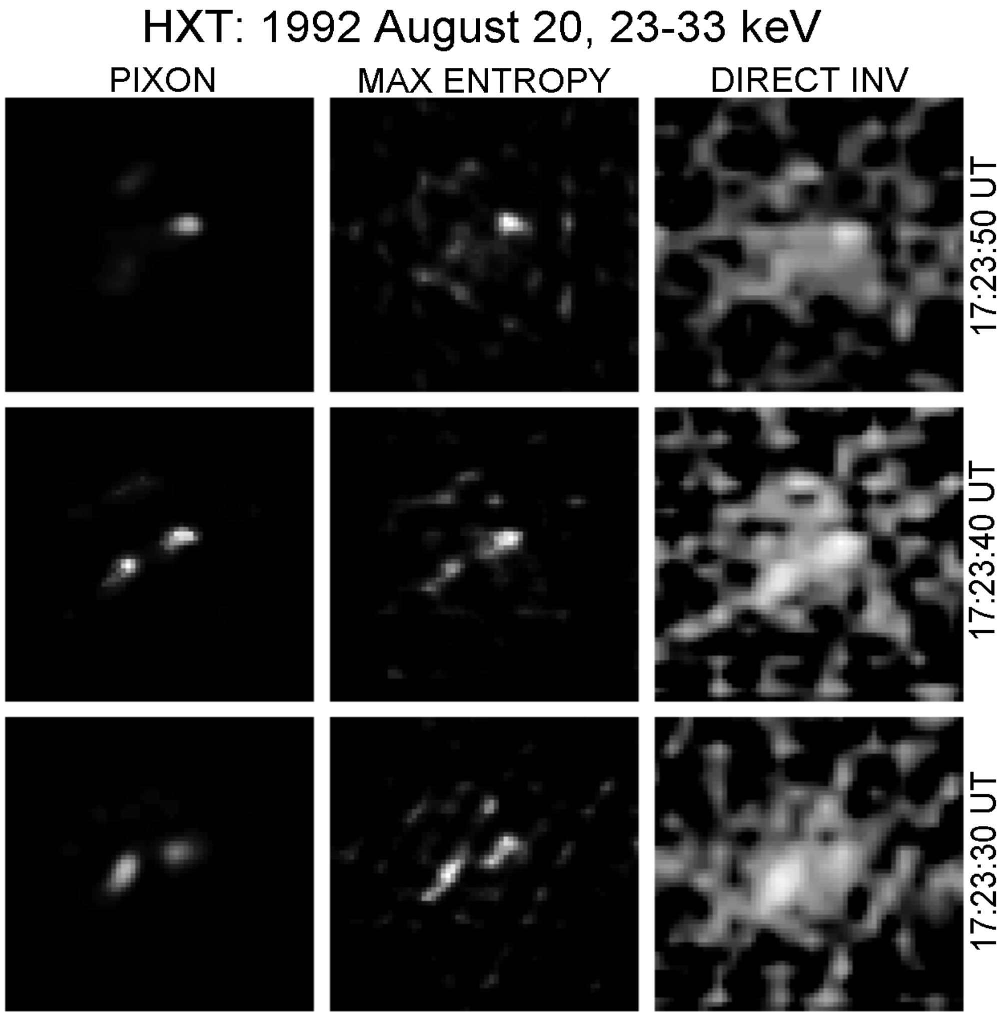


FIGURE 4. Hard X-ray (23-33 $keV$) images of the 20 August 1992 solar flare. The observations are from the hard X-ray Telescope (HXT) on board the Yohkoh satellite. Each column shows a time series of three image reconstructions. The background patterns which show up in the direct inversion and the ME inversion are artifacts resulting from the sparse UV-plane coverage in the HXT instrument. The pixon-based reconstruction essentially eliminates all of these artifacts. The reconstruction were performed by Metcalf of the University of Hawaii. Figure reproduced from Puetter 1995.

$3.8^\circ \times 11.4^\circ$ (FWHM). Each detector is mounted on an independent single-axis pointing system which allows for sub-stepping the detector field of view. Figure 5 presents a comparison of a pixon-based reconstruction of the OSSE survey data with the Non-Negative Least-Squares (NNLS) method developed at UCR. Both the NNLS and pixon-based reconstruction presented in Figure 7 were performed by D. Dixon of UC, Riverside (Dixon et al. 1996). Details of the UC, Riverside implementation of the pixon-based algorithm are given below. The dark area of the figure represents all of the points for which there is significant exposure time during the scanned observation. Each of the pixels in the reconstructed images in Figure 5 has an angular size of $2^\circ \times 2^\circ$.

As can be seen from Figure 5, the NNLS reconstruction produces an image which has the appearance of a random noise field. From this image, it is unclear whether

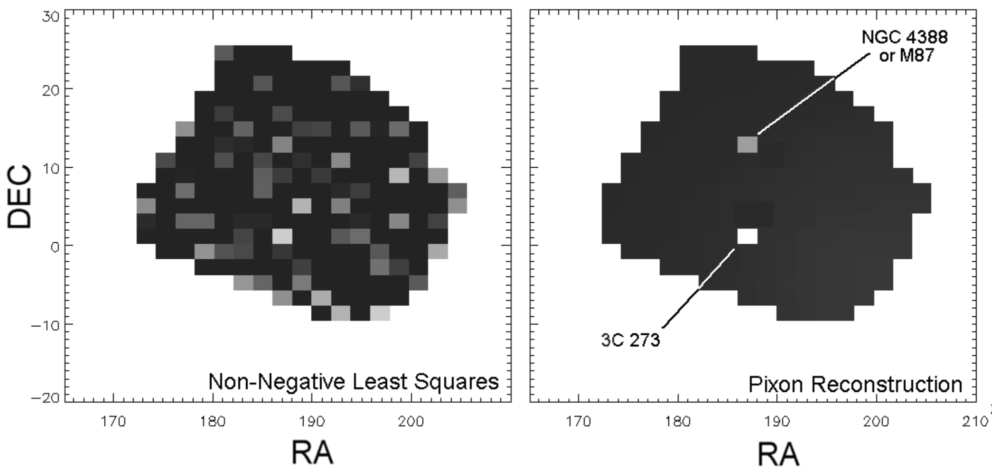


FIGURE 5. Non-Negative Least Squares (NNLS) and pixon-based image reconstructions from the 50-150 $keV$ data of the OSSE Virgo Survey. The reconstructions were performed by Dixon of the University of California, Riverside. While the NNLS method gives a result that looks like random noise, Dixon's simulated annealing, pixon-based method clearly reveals the two strong sources expected in these data, i.e. NGC 4388 and 3C 273. It also detects a mild gradient in the $\gamma$-ray background. Figure reproduced from Puetter 1995.

or not there are any real detections of sources. On the other hand, the pixon-based reconstruction clearly finds the two bright sources expected to be seen in this data, i.e. 3C273 and NGC 4388 (the active galaxy M87 is also in the pixel occupied by NGC 4388, but is not believed to contribute significant 50-150 $keV$ emission), and it can be seen that the pixon-based method was very successful in suppressing spurious sources in the reconstruction.

The OSSE data, and $\gamma$-ray data in general, present an especially difficult challenge for image reconstruction methods. This is because the signal-to-noise of the collected data is very low. At $\gamma$-ray energies there are only very few photons to count. Consequently the standard pixon-based methods developed at UCSD were found to be inadequate—the conjugate gradient method could not find the global minimum. It was for this reason that D. Dixon (U.C., Riverside) decided to use a simulated annealing approach to finding the optimal pixon reconstruction. As previously discussed, simulated annealing is well known for its robust ability to find shallow global minima in the presence of numerous local minima. However, this ability has significant computational costs. To speed the method, Dixon adopted a mean field approach and used only two pixon scales, one appropriate for point sources and one appropriate for the diffuse background. Given the expected nature of the image, this is quite a suitable assumption and gives rise to the excellent reconstruction presented in Figure 5. It is clear from the success of this method, that pixon-based approaches such as that of Dixon et al. (Dixon et al. 1996) have dramatically increased the scientific capability of the OSSE instrument. Current plans at UC, Riverside are to apply these techniques to COMPTEL data as well, and to explore simulated annealing pixon-based approaches with multiple pixon scales.

## 4. Conclusions

This lecture has presented a number of applications of pixon-based methods to the reconstruction of complexly encoded images. Comparisons of the performance of pixon-based techniques to other methods demonstrate that pixon-based methods provide consistently superior solutions with greater spatial resolution and sensitivity to faint sources. In addition, unlike other methods, pixon-based techniques robustly reject spurious sources. We have also discussed the special problems associated with complexly encoded images, i.e. a highly complex solution space with many local minima. Such problems typically have very small radii of convergence for standard multi-dimensional optimization methods (e.g. methods that approximate the optimization criterion as a quadratic form). Alternative, stochastic methods for solving the inverse problem were discussed, and a practical example of a simulated annealing, pixon-based reconstruction was given, i.e. the reconstruction of OSSE Virgo Survey data.

## 5. Acknowlegements

The author would like to thank a number of people for their valuable contributions to this work. Special thanks go to T. Metcalf (U. of Hawaii) and D. Dixon (U.C., Riverside) for extending the application of pixon-based methods to Yohkoh X-ray and GRO $\gamma$-ray data.

REFERENCES

Bontekoe, T. R. 1991, The Image Reconstruction Contest, in *Maximum Entropy and Bayesian Methods*, eds. W. T. Grady, Jr., and L. H. Schick, Kluwer Academic.

Bontekoe, T. R., Kester, D. J. M., Price, S. D., de Jonge, A. R. W., and Wesselieus, P. R. 1991, Image Reconstruction from the IRAS Survey, *Astron. and Astrophys.*, **248**, pp. 328-336. eds. W. T. Grady, Jr., and L. H. Schick, Kluwer Academic.

Cerny, V. 1982, A Thermodynamical Approach to the Traveling Salesman Problem: An Efficient Simulation Algorithm, preprint, Inst. Phys. and Biophys., Comenius Univ., Bratislava.

Conrad, M. 1974, Evolutionary Learning Circuits, *J. Theo. Bio.*, **46**, pp. 167-188.

Conrad, M. 1984, Microscopic-Macroscopic Interface in Biological Information Processing, *BioSystems*, **13**, pp. 303-320.

Conrad, M. 1988, Prolegomena to Evolutionary Programming, in *Advances in Cognitive Science: Steps toward Convergence*, eds. M. Kochen and H. M. Hastings, AAAS Selected Symposium, pp. 150-168.

Dixon, D. D., Tumer, O. T., Kurfess, J. D., Purcell, W. R., Wheaton, W. A., Piña, R. K., and Puetter, R. C. 1996, Pixon-Based Image Reconstruction from OSSE Data, *Ap. J.*, submitted.

Fogel, D. B. 1995, *Evolutionary Computation*, IEEE Press.

Fraser, A. S. 1957a, Simulation of Genetic Systems by Automatic Digital Computers. I. Introduction, *Australian J. of Biol. Sci.*, **10**, pp. 484-491.

Fraser, A. S. 1957b, Simulation of Genetic Systems by Automatic Digital Computers. I. Effects of Linkage on Rates of Advance Under Selection, *Australian J. of Biol. Sci.*, **10**, pp. 492-499.

Fraser, A. S. 1968, The Evolution of Purposive Behavior, in *Purposive Systems*, eds. H. von Foerster, J. D. White, L. J. Peterson, and J. K. Russell, pp. 15-23, Spartan Books.

German, S., and German, D. 1984, Stochastic Relaxation, Gibbs Distributions, and the Bayesian Restoration of Images, *IEEE Trans. Pat. Anal. and Mach. Intel.*, **PAMI-6(6)**, pp. 721-741.

Hardle, W. 1990, *Applied Non-Parametric Regression*, Econometric Society Monographs, Cambridge University Press.

HEDEN, H. 1975, *Non-Parametric Emperical Bayes Estimation*, Arboga.

HOLLAND, J. H. 1969, Adaptive Plans Optimal for Payoff-Only Environments, in *Proc. of the Second Hawaii Intern. Conf. on Sys. Sciences*, pp. 917-920.

HOLLAND, J. H. 1975, *Adaptation in Natural and Artificial Systems*, University of Michigan Press.

KAMPFNER, R. P., AND CONRAD, M. 1983, Computational Modeling of Evolutionary Learning Processes in the Brain, *Bull. Math. Bio.*, **45**, pp. 931-968.

KIRKPATRICK, S., GELATT, C. D., AND VECCHI, M. P. 1983, *Science*, **220**, pp. 671-680.

KIRKPATRICK, S. 1984, *J. Stat. Phys.*, **34**, pp. 975-986.

KOSUGI, T., MAKISHIMA, K., MURAKAMI, T., SAKAO, T., AND OTHERS 1991, The Hard X-Ray Telescope (HXT) for the Solar-A Mission, *Solar Phys.*, **136**, pp. 17-36.

METCALF, T. R., HUDSON, H. S., KOSUGI, T., PUETTER, R. C., AND PIÑA, R. K. 1996, Pixon-Based Multiresolution Image Reconstruction for Yohkoh's Hard X-ray Telescope, *Ap. J.*, in press.

PUETTER, R. C., 1995, Pixon-Based Multiresolution Image Reconstruction and the Quantification of Picture Information, *Int. J. of Imaging Sys. and Tech.*, **6**, pp. 314-331.

PUETTER, R. C., AND PIÑA, R. K., 1993a, Beyond Maximum Entropy: Fractal Pixon-Based Image Reconstruction, in *Proc. Science with High Spatial Resolution Far-Infrared Data*, IPAC, 14-16 June 1993.

PUETTER, R. C., AND PIÑA, R. K., 1993b, Pixon-Based Image Reconstruction, in *Proc. MaxEnt 93*, UCSB, 1-5 August 1993.

PRESS, W. H., TEUKOLSKY, S. A., VETTERING, W. T., AND FLANNERY, B. P. 1994, *Numerical Recipes in C: The Art of Scientific Computing*, second edition, third printing, Cambridge University Press.

RICE, W. 1993, An Atlas of High-Resolution IRAS Maps of Nearby Galaxies, *A. J.*, **105**, pp. 67-96.

SPRENT, P. 1981, *Quick Statistics: An Introduction to Non-Parametric Methods*, Penguin Books.

VAN DE HULST, J. M., KENNICUTT, R. C., CRANE, P. C., AND ROTS, A. H. 1988, Radio Properties and Extinction of the H II Regions in M51, *Astron. and Astrophys.*, **195**, pp. 38-52.

WEIR, N. 1993, private communication.